Science and Technology Indonesia
e-ISSN:2580-4391 *p*-ISSN:2580-4405
Vol. 9, No. 3, July 2024

Research Paper

Europium-Subsituted Bismuth-Based Superconductors: Structural and Thermal Analysis via Chemical Sol-Gel Synthesis

Firas Salim Abed[1]*, Lamia K. Abbas[1]

[1]*Department of Physics, College of Science, University of Baghdad, Baghdad, 10070, Iraq*
***Corresponding author**: firas.abd2204p@sc.uobaghdad.edu.iq*

Abstract
The synthesis and characterization of $Bi_{1.7-x}Pb_{0.3}Eu_xSr_2Ca_2Cu_3O_{10+\delta}$ superconductors with Eu substitution at varying ratios were investigated to determine their structural, electrical, and thermal properties. A sol-gel technique followed by calcination was employed to prepare samples with different substitution ratios. X-ray diffraction (XRD) was used for structural analysis, electrical properties with aid of nitrogen fluid measured by electrical resistivity, thermogravimetric analysis (TGA) conducted for thermal properties , and differential scanning calorimetry (DSC) were utilized for characterization" to improve clarity. XRD analysis revealed that the highest proportion of the high-temperature superconducting (HTS) phase occurred at a substitution factor of 0.2, corresponding to the highest critical temperature (Tc) value of 112 K. Raman spectra were conducting and showed a certain shifting with different substitution levels of Eu element. The thermal analysis highlighted the impact of substitution factor x on thermal stability, with the sample at x=0.2 exhibiting the highest thermal stability. TGA curves showed mass loss behavior for different x values, with distinct regions indicating the presence of residuals. The successful synthesis and characterization of these superconductors hold promise for practical applications.

Keywords
BSCCO, High Tc Phase, Sol-Gel, DSC, TGA

Received: 19 March 2024, Accepted: 17 May 2024
https://doi.org/10.26554/sti.2024.9.3.621-628

1. INTRODUCTION

High-temperature superconducting ceramics have garnered significant attention due to their potential applications (Sam et al., 2019). Extensive research has been devoted to understanding and optimizing the superconducting properties of these materials (Fallah Arani et al., 2018). However, challenges persist in the fabrication process of such ceramics (Stryczewska et al., 2022). Cuprates remain the most promising candidates for various applications (Muhammed and Abbas, 2023), primarily due to their high critical temperature (Tc) (Shimoyama and Motoki, 2024). Among these materials, $Bi_2Sr_2Ca_2Cu_3O_{10+\delta}$ (Bi-2223) has emerged as particularly suitable for numerous applications. The Bi-2223 phase coexists with the lower-phase Bi-2212 (Tc < 96 K) (Polasek et al., 2004). Notably, introducing substitution elements in specific ratios for each cation can lead to variations in the electronic and magnetic properties of the BSCOO superconductor, including its critical temperature (Tc) (Agwamba et al., 2023).

BSCCO superconductors can manifest as Bi-2201, Bi-2212, and Bi-2223 phases, with Bi-2223 exhibiting the highest transition temperature (Tc) (Mohammed and Jasim, 2018). However, achieving pure-phase or single-crystal Bi-2223 is challenging (Qiu et al., 2021). Efforts are underway to enhance the superconducting properties by increasing the high-temperature superconducting (HTS) ratio through various techniques (O'Mahony et al., 2022). The conventional method for producing ceramic superconductors involves a solid-state thermochemical reaction, wherein powders are mixed at specific molar ratios (Antoncik et al., 2020). An alternative approach utilizing sol-gel processes aims to create a homogeneous mixture, facilitating the uniform distribution of metal ions at stoichiometric ratios (Zhao et al., 2023). Studies suggest that partial substitution of Bi with Pb can accelerate phase formation kinetics and enhance the yield of the Bi-2223 phase through partial melting of Pb-doped samples (Maljuk and Lin, 2016).

To comprehend the crystallization kinetics and thermal stability, crucial for BSCOO superconductor preparation, thermal analysis techniques such as differential thermal analysis (DTA) and differential scanning calorimetry (DSC) have been extensively investigated (Mayoral et al., 2004). Raman shifting can also utilized to identify the superconductor molecule dynamics for pure BSCCO (Rodrigues et al., 2017).

This study aims to synthesize Eu-substituted BSCCO superconductors with improved superconducting properties by optimizing the substitution ratio using the Sol-gel technique. The investigation involves analyzing the structural, electrical, and thermal characteristics of samples with varying Eu-substitution ratios. Characterization of the synthesized samples entails a detailed analysis to determine structural parameters and the ratio of high-temperature superconducting (HTS) phase. Additionally, the study examines the variation of critical temperature (Tc) and the thermal properties behavior at different dopant ratios. Finally, the Raman spectra were conducted to study the vibrational modes of the BSCCO molecule with different Eu substitution levels.

2. EXPERIMENTAL SECTION

2.1 Materials

The starting materials, including bismuth nitrate pentahydrate $Bi(NO_3)_2.5H_2O$, lead nitrate $Pb(NO_3)_2$, europium nitrate $Eu(NO_3)_2$, sintrontium nitrate $Sr(NO_3)_2$, calcium nitrate quadr ahydrate $Ca(NO_3)_2.4H_2O$, and cuprate nitrate trihydrate $Cu(NO_3)_2.3H_2O$. Nitric acid HNO_3 was used as catalyst. Ethylenediaminetetraacetic acid (EDTA), ethylene glycol (EG), and urea were employed as a complexing agent, binding agent, and fuel, respectively.

2.2 Instruments

The prepared samples were subjected to x-ray diffraction (XRD) analysis (SHIMADZU) to investigate their structural properties. Electric characterization was performed using the dc four-probe method to determine the critical temperature for each sample, aided by liquid nitrogen. The Raman spectra wrere collected in order to obtain valuable information about the vibrational modes and the bonding between the atoms in the superconducter material. Thermal analysis was conducted using differential scanning calorimetry (DSC) and thermogravimetric analysis (TGA).

2.3 Methods

The synthesis procedure for Bismuth-based superconductor samples with the general formula $Bi_{1.7-x}Pb_{0.3}Eu_xSr_2Ca_2Cu_3O_{10+\delta}$ was carried out via the chemical sol-gel method. The starting materials, including $Bi(NO_3)_2.5H_2O$, $Pb(NO_3)_2$, $Eu(NO_3)_2$, $Sr(NO_3)_2$, $Ca(NO_3)_2.4H_2O$, and $Cu(NO_3)_2.3H_2O$, were used in specified molar ratios corresponding to the substitution factor (x) ranging from 0 to 0.5 (EDTA), (EG), and urea were employed as a complexing agent, binding agent, and fuel, respectively.

Initially, the starting materials were mixed in distilled water according to the molar ratios specified by the formula $Bi_{1.7-x}Pb_{0.3}Eu_xSr_2Ca_2Cu_3O_{10+\delta}$ for various values of x. The resulting mixture was stirred at 45°C, and EG was dissolved in a specific volume of distilled water, which was then combined with EDTA to induce precipitation. The pH was adjusted at 7 by adding gradually ammonium hydroxide (NH_3OH) at 60°C, resulting in the elimination of precipitation and transformation of the solution into a gel. This gelation process was repeated for subsequent samples, and the formed gel was further treated by the addition of urea.

The gel was dried on a hot plate with gradual heating from 60 to 250°C in air, yielding a black-gray powder over 72 hours. To remove residual nitrates and oxides, a calcination procedure was conducted for six hours at 800°C, resulting in the formation of the final black BSCCO powder. This powder was then homogenized using a gate mortar for half an hour. Subsequently, pellets were prepared from the powder samples using a hydraulic piston at 10-ton pressure. The pellets underwent a sintering process at 850°C for 48 hours, to be ready for subsequent characterization.

3. RESULTS AND DISCUSSION

The X-ray diffraction (XRD) patterns presented in Figure 1 elucidate the structural characteristics of $Bi_{1.7-x}Pb_{0.3}Eu_xSr_2Ca_2Cu_3O_{10+\delta}$ samples, wherein the parameter x undergoes variation due to Eu substitution. These specimens demonstrate a dual-phase constitution, primarily characterized by a tetragonal Bi-2223 phase and a secondary presence of the low-temperature Bi-2212 phase. The proportion of the high-temperature superconducting (HTS) phase experiences alteration with the partial substitution of Eu for Bi in the $Bi_{1.7-x}Pb_{0.3}Eu_xSr_2Ca_2Cu_3O_{10+\delta}$ compound. Moreover, faint unidentified peaks are discernible in the diffraction patterns. The determination of the HTS phase fraction was achieved through the summation of intensities for diffraction peaks corresponding to Bi-2212 and Bi-2223 (Zelati et al., 2014).

The analysis of the structural characteristics indicates an increase in the Bi-2232 phase, reaching a peak of 60.51% for x=0.2. Further increase in Eu substitution concentration beyond 0.2 causes a reduction in the percentage of the high-temperature phase (HTS), attributed to the decreased stability of the Bi-2223 phase (Sarun et al., 2008). The Eu substitution suggested the elevate of cuprite vacancies, leading to enhanced scattering of super-electrons within the crystalline lattice (Aljurani et al., 2021). The crystallographic structure of the prepared samples is determined to be orthorhombic, with lattice parameters a=5.4741 Å, b=5.2789 Å, and c=36.2179 Å (Khaleel and Abbas, 2023). The positions of diffraction peaks exhibit slight variations with variation in x values, indicating strain-induced alterations in lattice parameters, consistent with the observed changes in lattice constants. Details regarding the variations in lattice parameters (a, b, and c) with x values are presented in Table 1. Regarding the Eu-substituted samples, the c-lattice parameter demonstrates a similar trend to that observed in the percentage of the HTS percentage (Tuama and Abbas, 2021). This behavior correlates with the findings concerning HTS%. The distortion and fluctuation in the c-axis, attributed to substitution-induced discrepancies in ionic radii between Bi^{3+} (117 pm) and Eu^{3+} (108 pm) (Geoffrey N áCloke, 1993), significantly influencing the c parameter. Table 1 outlined the calculations of the c/a ratio and unit cell density (ρ) based on lattice parameters.

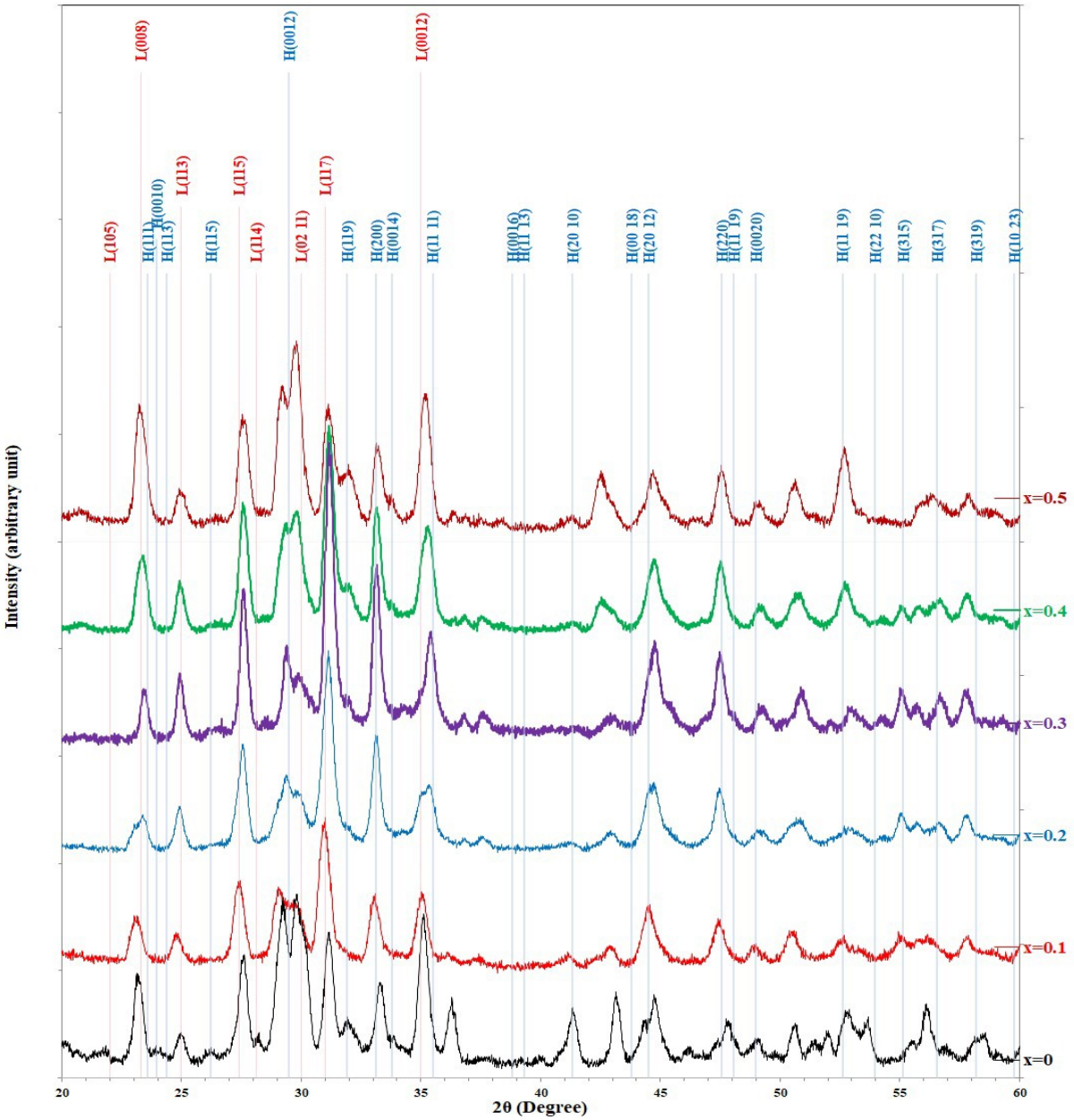

Figure 1. XRD Patterns for $Bi_{1.7-x}Pb_{0.3}Eu_xSr_2Ca_2Cu_3O_{10+\delta}$ at Different Eu Substitutions

The variation of HTS percentage and c/a ratio for $Bi_{1.7-x}Pb_{0.3}Eu_xSr_2Ca_2Cu_3O_{10+\delta}$ samples with substitution factor x are displayed in Figure 2. The two patterns show a nearly analogous trend, reaching a peak value for HTS of 60.51% and a maximum c/a ratio of 6.63 at x=0.2.

The variation of electrical resistivity with decreasing temperature for $Bi_{1.7-x}Pb_{0.3}Eu_xSr_2Ca_2Cu_3O_{10+\delta}$ samples at different substitution factors (x) are displayed in Figure 3. The inset shows a notable decrease in resistivity as the temperature approaches the critical temperature (Tc), indicating the onset of superconducting behavior in the samples (de Vera et al., 2019). The transition to the superconducting state occurs wherein electrical resistance drops to zero, enabling the flow of electric current without energy loss (Abed and Jassim, 2019). The critical temperature values for each sample are provided in Table 2. Notably, the sample with x=0.2 exhibited the highest Tc value, reaching 112 K. This observation suggests that the substitution factor x influences the superconducting properties of the samples, with x=0.2 yielding the highest HTS phase ratio, causing the highest Tc value among the tested compositions (Jassem and Abed, 2019).

The Raman spectra of all prepared samples in the range

Table 1. Structural Parameters for $Bi_{1.7-x}Pb_{0.3}Eu_xSr_2Ca_2Cu_3O_{10+\delta}$

X	a (Å)	b (Å)	c (Å)	V (Å^3)	c/a	w (g/mole)	ρm (g/cm^3)	HTP %
0	5.4741	5.2789	36.2179	1046.593	6.6162	1023.454	6.4944	58.65%
0.1	5.5203	5.3183	36.7183	1078.004	6.6515	1017.752	6.2700	57.08%
0.2	5.5031	5.3315	36.4976	1070.832	6.6322	1012.051	6.2767	60.51%
0.3	5.5125	5.3180	36.3905	1066.796	6.6015	1006.349	6.2649	60.40%
0.4	5.5005	5.3191	36.4976	1067.837	6.6354	1000.648	6.2233	59.22%
0.5	5.4974	5.3168	36.4778	1066.204	6.6354	994.946	6.1974	59.77%

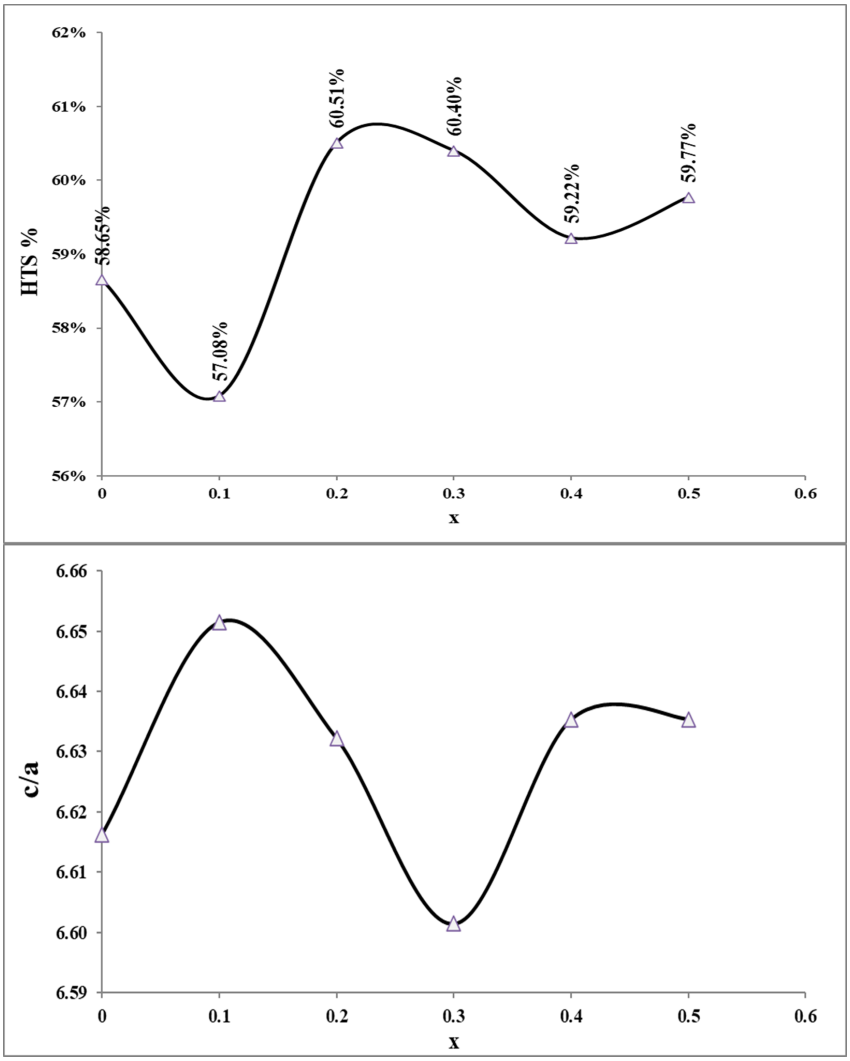

Figure 2. HTS Percentage, and c/a Versus x for $Bi_{1.7-x}Pb_{0.3}Eu_xSr_2Ca_2Cu_3O_{10+\delta}$

Table 2. Tc Values of $Bi_{1.7-x}Pb_{0.3}Eu_xSr_2Ca_2Cu_3O_{10+\delta}$ at Different Eu Substitutions

	x=0	x=0.1	x=0.2	x=0.3	x=0.4	x=0.5
Tc (K)	111	111	112	110	109	107

from 50 to 1000 cm^{-1} are showed in Figure 4. The Raman spectra of BSCCO are a powerful tool for understanding the electronic and structural properties as well as the lattice dynamics of high-temperature superconductors. Several peaks are shown by the spectrum which can be attribute to several vibrations of the BSCCO compound. Peaks at 140 cm^{-1} and 300 cm^{-1} are attributed to the vibrations of the CuO_2 planes and Bi−O bond respectively, the intensity of these peaks is sensitive to the oxygen content and the substitution levels in the material. Peaks at 500 cm^{-1} and 600 cm^{-1} are associated

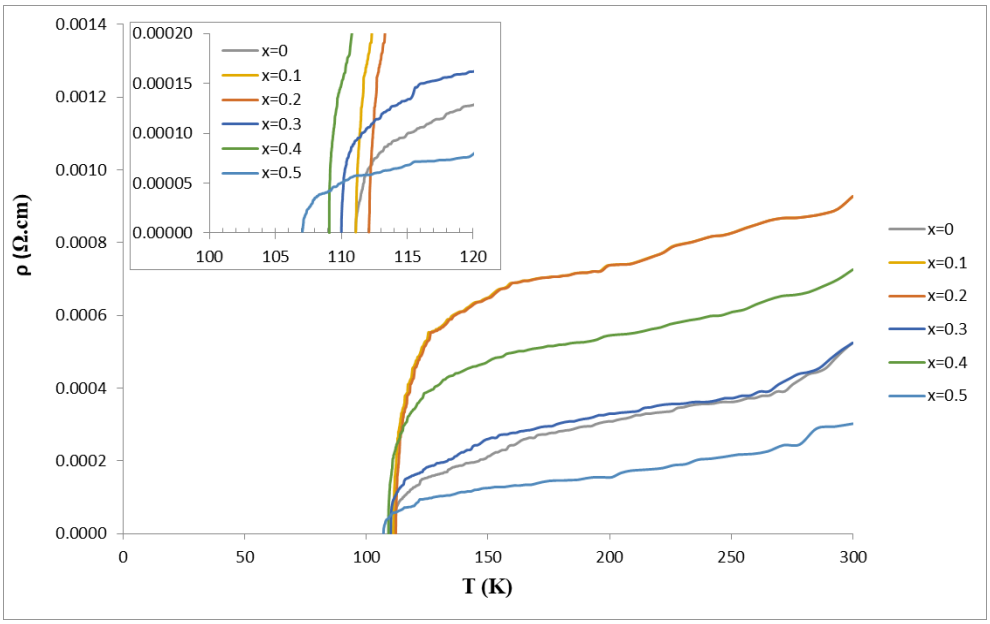

Figure 3. Resistivity vs Temperature of $Bi_{1.7-x}Pb_{0.3}Eu_xSr_2Ca_2Cu_3O_{10+\delta}$ at Different Eu Substitutions

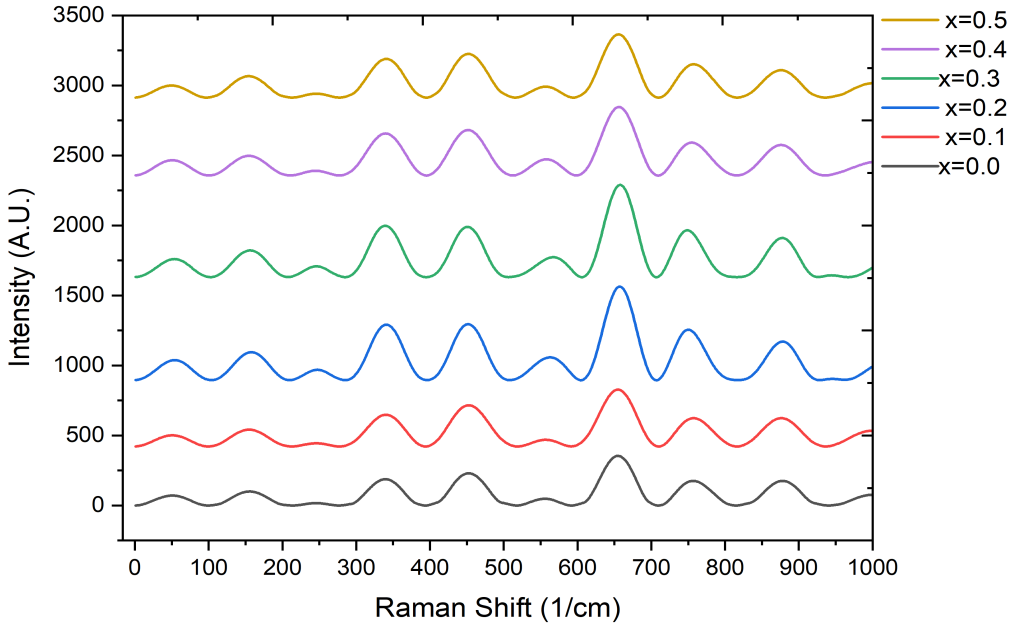

Figure 4. Shows the Raman Spectra of $Bi_{1.7-x}Pb_{0.3}Eu_xSr_2Ca_2Cu_3O_{10+\delta}$ at Different Eu Substitutions

with the vibrations of the Sr−O the Ca−O bonds respectively in the material. The intensity of these peaks is relatively constant across different oxygen content and substitution levels. While Peaks at 800 cm^{-1} and 1000 cm^{-1} are attributed to the vibrations of the Cu−O and Bo−O bonds respectively in the material (Figueruelo Campanero et al., 2024). The intensity of these peaks is sensitive to the oxygen content and the substitution levels. Substitution of Pb and different x values of europium elements in the $Bi_{1.7-x}Pb_{0.3}Eu_xSr_2Ca_2Cu_3O_{10+\delta}$ superconductor matrix leads to rise of some additional peaks. There is also a significant shift in Raman modes with different substitution levels.

Thermal analysis was conducted on the prepared samples, specifically the Differential Scanning Calorimetry (DSC) and

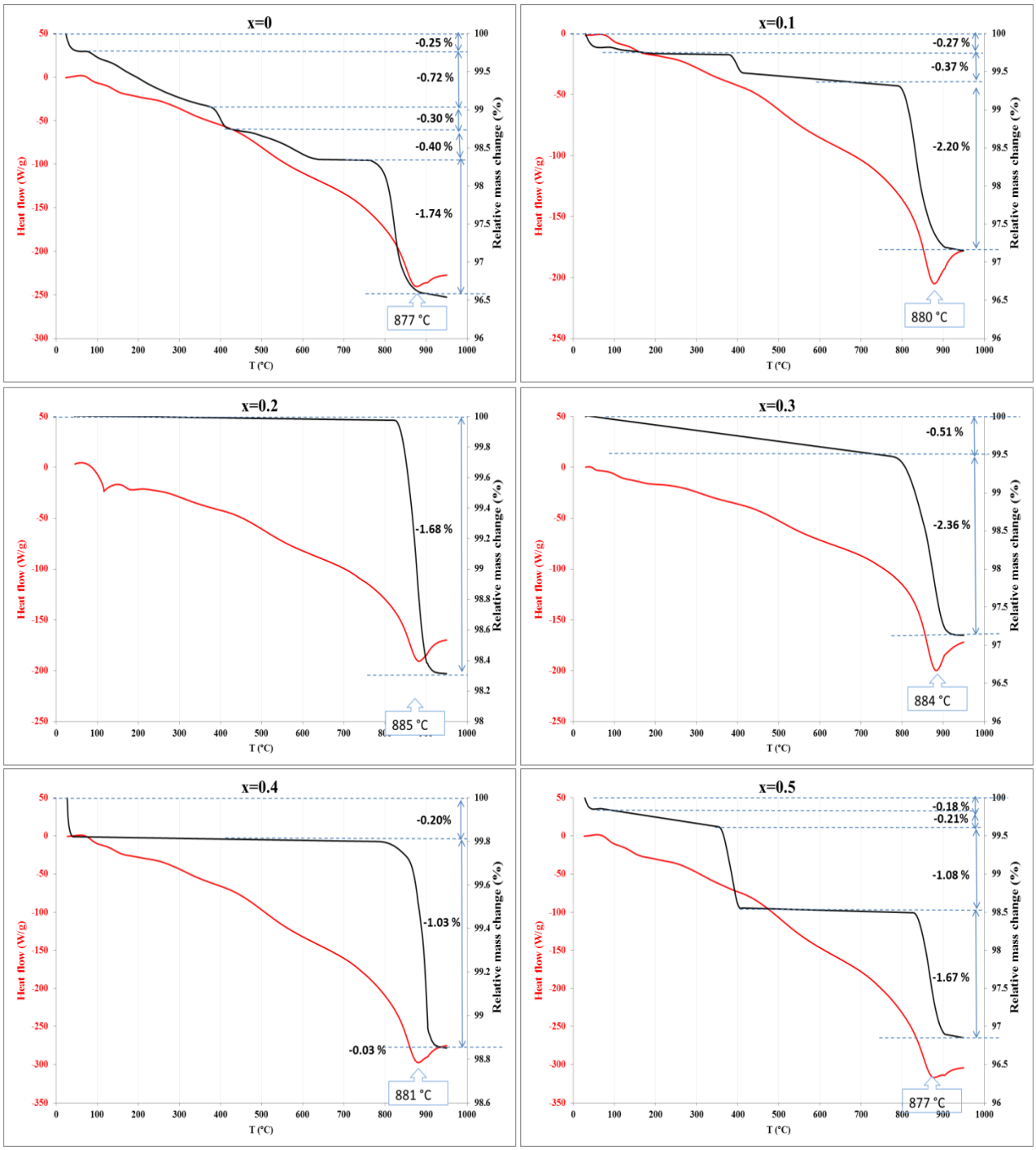

Figure 5. DSC and TGA Curves of $Bi_{1.7-x}Pb_{0.3}Eu_xSr_2Ca_2Cu_3O_{10+\delta}$ at Different Eu Substitutions

Thermogravimetric Analysis (TGA) of $Bi_{1.7-x}Pb_{0.3}Eu_xSr_2Ca_2Cu_3O_{10+\delta}$, in the temperature range of 23°C–950°C, to investigate the melting behaviors and mass loss during heating process. In Figure 5, the DSC curves exhibit a prominent endothermic peak, which has been identified as the melting point of Bi-2212 (Jin et al., 2023). The position of this peak varies with the substitution factor x. For instance, for the sample with x=0, the endothermic peak appears at 877°C. However, as x increases to 0.2, the starting melting point shifts slightly to a higher temperature of 885°C. This shift is attributed to the influence of the highest ratio of the 2223 phase at x=0.2, indicating an enhancement in thermal stability (Zhao et al., 2019). Further increase in the value of x causes a slight retardation of the endothermic peak to a lower temperature. This observa-

Table 3. Mass Loss for Different Temperature Ranges of $Bi_{1.7-x}Pb_{0.3}Eu_xSr_2Ca_2Cu_3O_{10+\delta}$ at Different Eu Substitutions

Temp. Range (°C)	Mass loss %					
	x=0	x=0.1	x=0.2	x=0.3	x=0.4	x=0.5
30-100	-0.25	-0.27	-	-	-0.2	-0.18
100-380	-0.72	-	-	-	-	-0.21
380-420	-0.3	-0.37	-	-	-	-1.08
420-800	-0.4	-	-	-0.51	-	-
800-900	-1.74	-2.2	-1.68	-2.36	-1.03	-1.67

tion suggests that as x increases beyond 0.2, there might be a change in the composition or structure of the sample, affecting its thermal properties (Kavitha et al., 2024). Moreover, the intensity of the endothermic peak is found to vary depending on the ratio of the low phase (2212). It is noted that the lowest appearance of the peak is observed at x=0.2, while it becomes more significant both below and above this ratio. This variation in intensity further indicates the influence of the composition on the melting behavior of the samples.

The TGA curves show many regions for mass loss. The initial region of low percentage mass loss, typically occurring up to around 100°C, corresponds to the desorption of physically adsorbed moisture from the sample surface. The extent of moisture loss can vary among samples depending on factors such as their hygroscopic nature or porosity. The multiple regions appeared from 100 to 800°C corresponding the existence to some residuals of metal nitrates or carbonates (Jin et al., 2023). These substances of low content decompose on heating to give metal oxide, nitrogen dioxide (NO_2), and carbon dioxide (CO_2) cause small mass lose in the sample (Xingming et al., 2020). The decomposition temperatures of metal nitrates can vary depending on the specific metal, so different stages of decomposition at different temperatures appear according to their types (Polasek et al., 2004). The final region appeared at the temperature ranges higher than 800°C of a significant mass loss. During melting process of the 2212 phase some of their molecules decompose into its constituent elements or undergo structural changes, leading to a loss in mass or oxygen loss from the lattice structure. The comparison between the samples of different Eu substitution, show that the sample of x=0.2 has single range of mass loss at decomposition temperature higher than 800°C indicate its purity than the nitride phases and its low moisture content. This sample appeared with lower mass percentage loss at this region(1.68%) indicate its lower content of the 2212 corresponding to the 2223 phase.

Mass loss and their temperature ranges of $Bi_{1.7-x}Pb_{0.3}Eu_xSr_2Ca_2Cu_3O_{10+\delta}$ at different content of Eu substitutions are listed in Table 3.

4. CONCLUSION

Characterization techniques for the prepared samples including XRD, DSC, and TGA were employed. XRD analysis revealed that the highest percentage of high-temperature superconducting (HTS) phase occurred at a substitution factor of 0.2, consistent with the variation in the c/a ratio. Specifically, the sample with x=0.2 demonstrated the highest critical temperature (Tc) value, indicating the significant influence of the substitution factor on superconducting properties, with an optimal Tc of 112 K. Raman spectra showed a certain shifting in the vibrational modes and increasing in intensity with various levels of substitution which is largly for the x=0.2. Thermal analysis provided insights into the melting behaviors of the $Bi_{1.7-x}Pb_{0.3}Eu_xSr_2Ca_2Cu_3O_{10+\delta}$ samples, highlighting the impact of the substitution factor on thermal stability and composition-dependent variations in melting characteristics. Notably, the sample at x=0.2 exhibited the highest thermal stability. TGA curves exhibited mass loss behavior for different x values, with multiple regions observed between 100 and 800°C, suggesting the presence of some residuals in the samples. However, nearly pure samples, in addition to the lowest mass loss at the melting point of the 2122 phase, are indicative of a lower ratio of this phase in these samples. Sample with x=0.2 showed a single range of mass loss at a decomposition temperature higher than 800°C.

5. ACKNOWLEDGMENT

We would like to express my special thanks to Dr. Amal Kadhum Jasim and o Mr. Mohanad A. Aswad for their support.

REFERENCES

Abed, F. S. and A. K. Jassim (2019). Co-Doping Effect (Pb and Nd) on Mechanical Properties of BSCCO System. *Indian Journal of Natural Sciences*, **9**(52); 16281–16286

Agwamba, E. C., I. J. Mbonu, Y. N. Kavil, G. E. Mathias, A. M. Bakheet, O. J. Ikenyirimba, I. Hossain, M. C. Muozie, T. E. Gber, and H. Louis (2023). Superconductivity, Quantum Capacitance, and Electronic Structure Investigation of Transition Metals (X= Y, Zr, Nb, Mo) Encapsulated Silicon Nanoclusters ($Si_{59}X$): Intuition from Quantum and Molecular Mechanics. *Materials Today Communications*, **37**(December); 107498

Aljurani, B., G. Hermiz, and M. Alias (2021). Superconductivity Measurements of (Hg, Ti)-1223 Compound Prepared in Capsule. *Iraqi Journal of Science*, **62**(9); 2934–2939

Antoncik, F., O. Jankovsky, T. Hiasek, and V. Bartunek (2020). Nanosized Pinning Centers in the Rare Earth-Barium-Copper-Oxide Thin-Film Superconductors. *Nanomaterials*, **10**(8); 1429

de Vera, F. I., H. Bardolaza, C. Arcilla, and R. Sarmago (2019). Effect of In_2O_3 on the grain connectivity and superconducting behavior of $Bi_2Sr_{2-x}In_xCaCu_2O_{8+d}$. *SN Applied Sciences*, **1**(96); 1–8

Fallah Arani, H., S. Baghshahi, A. Sedghi, D. Stornaiuolo, F. Tafuri, and N. Riahi-Noori (2018). Enhancement in Superconducting Properties of $Bi_2Sr_2Ca_1Cu_2O_{8+\theta}$ (Bi-2212) by Means of Boron Oxide Additive. *Physica C: Superconductivity and Its Applications*, **548**(May); 31–39

Figueruelo Campanero, I., A. del Campo, G. Nieva, E. M. González, A. Serrano, and M. Menghini (2024). Apparent Color and Raman Vibrational Modes of the Unconventional Superconductor $Bi_2Sr_2CaCu_2O_{8+\delta}$ Exfoliated Flakes. *ArXiv Preprint ArXiv*, **2402**(12941); 1–10

Geoffrey N áCloke, F. (1993). Zero Oxidation State Compounds of Scandium, Yttrium, and the Lanthanides. *Chemical Society Reviews*, **22**(1); 17–24

Jassem, A. and F. S. Abed (2019). Enhancement of Tc by Substitution of (Pb and Nd) in Bismuth-Based High-Tc Superconductors Material. *Journal of Non-Oxide Glasses*, **11**(3); 41–47

Jin, L., G. Liu, J. Feng, X. Xu, G. Jiao, S. Zhang, Q. Hao, P. Zhang, and C. Li (2023). Dominant Effect of Residual Secondary Phase of Powders on Jc and Microstructure of Bi-2212 Superconducting Wires. *Superconductivity*, **8**(December); 100060

Kavitha, M., S. Sarvesh, M. Arshad, M. Surendar, and G. Ragavan (2024). Effect of Ba and Mg Substitution on the Phase Formations of Combustion Synthesized BSCCO Superconductor. *Journal of The Institution of Engineers (India): Series D*, **557**(2); 1–7

Khaleel, A. K. and L. K. Abbas (2023). Synthesis and Characterization of PVDF/PMMA/ZnO Hybrid Nanocomposite Thin Films for Humidity Sensor Application. *Optik*, **272**(February); 170288

Maljuk, A. and C. Lin (2016). Floating Zone Growth of $Bi_2Sr_2Ca_2Cu_3O_y$ Superconductor. *Crystals*, **6**(5); 62

Mayoral, M., J. Andrés, M. Bona, L. Angurel, and E. Natividad (2004). Approximation to the Laser Floating Zone Preparation of High Temperature BSCCO Superconductors by DSC. *Thermochimica Acta*, **409**(2); 157–164

Mohammed, L. A. and K. A. Jasim (2018). Synthesis and Study the Structural and Electrical and Mechanical Properties of High Temperature Superconductor Tl0. 5pb0. 5ba2can-1cun-Xnixo2n+ 3-Î´ Substituted with Nickel Oxide for N= 3. *Ibn AL-Haitham Journal For Pure and Applied Sciences*, **31**(3); 26–32

Muhammed, S. A. and N. K. Abbas (2023). Synthesis and Investigation of Structural and Optical Properties of CdO:Ag Nanoparticles of Various Concentrations. *Baghdad Science Journal*, **20**(5 (Suppl.)); 2002–2011

O'Mahony, S. M., W. Ren, W. Chen, Y. X. Chong, X. Liu, H. Eisaki, S. i. Uchida, M. Hamidian, and J. S. Davis (2022). On the Electron Pairing Mechanism of Copper-Oxide High Temperature Superconductivity. *Proceedings of the National Academy of Sciences*, **119**(37); e2207449119

Polasek, A., P. Majewski, E. T. Serra, F. Rizzo, and F. Aldinger (2004). Phase Relations Study on the Melting and Crystallization Regions of the Bi-2223 High Temperature Superconductor. *Materials Research*, **7**(3); 393–408

Qiu, D., C. Gong, S. Wang, M. Zhang, C. Yang, X. Wang, and J. Xiong (2021). Recent Advances in 2D Superconductors. *Advanced Materials*, **33**(18); 2006124

Rodrigues, V. D., G. A. d. Souza, C. L. Carvalho, and R. Zadorosny (2017). Effect of La Doping on the Crystal Structure, Electric, Magnetic and Morphologic Properties of the BSCCO System. *Materials Research*, **20**(5); 1406–1413

Sam, C., M. Mosbah, S. Attaf, and N. Benbellat (2019). The Effect of Ba Doping on Sr Site on Structural and Superconducting Properties of Bi2212 Phase. *Physica B: Condensed Matter*, **557**(March); 12–16

Sarun, P., S. Vinu, R. Shabna, A. Biju, and U. Syamaprasad (2008). Highly Enhanced Superconducting Properties of Eu-Doped (Bi, Pb)-2212. *Materials Letters*, **62**(17-18); 2725–2728

Shimoyama, J. i. and T. Motoki (2024). Current Status of High Temperature Superconducting Materials and their Various Applications. *IEEJ Transactions on Electrical and Electronic Engineering*, **19**(3); 292–304

Stryczewska, H. D., M. A. Stępień, and O. Boiko (2022). Plasma and Superconductivity for the Sustainable Development of Energy and the Environment. *Energies*, **15**(11); 4092

Tuama, M. J. and L. K. Abbas (2021). Superconducting Properties of $Bi_{2-x}Pb_{0.3}W_xSr_2Ca_2Cu_3O_{10+\delta}$ Compounds. *Iraqi Journal of Science*, **62**(2); 490–495

Xingming, Z., D. Wang, T. Wang, H. Songchol, L. Jiang, D. Yuxiang, and Q. Yang (2020). Preparation of $Bi_2Sr_2CaCu_2O_{8+\delta}$ (Bi2212) Superconductor by Pechini Sol–Gel Method: Thermal Decomposition and Phase Formation Kinetics of the Precursors. *Journal of Materials Science. Materials in Electronics*, **31**(22); 19997–20008

Zelati, A., A. Amirabadizadeh, A. Kompany, H. Salamati, and J. Sonier (2014). Effect of Eu_2O_3 Nanoparticles Addition on Structural and Superconducting Properties of BSCCO. *Journal of Superconductivity and Novel Magnetism*, **27**(6); 1369–1379

Zhao, X., Z. Lv, Y. Qi, X. Lu, W. Wei, D. Ma, W. Gong, F. Wu, and T. Wang (2023). A Process for the Preparation of High-Quality and Uniform Large-Scale Bi2212 Superconducting Films Via the Sol-Gel Method. *Journal of Materials Research and Technology*, **26**(September-October); 8337–8350

Zhao, X., T. Wang, S. Hong, D. Sun, N. Wang, G. Chae, and Y. Qi (2019). Superconducting Properties and Non-Isothermal Crystallization Kinetics of a $Bi_2Sr_2CaCu_2O_{8+\delta}$ (bi2212) Superconductor Prepared by the Pechini Sol–Gel Method. *RSC Advances*, **9**(60); 35280–35288

